Improving Glass-Fiber Epoxy Composites via Interlayer Toughening with Polyacrylonitrile / Multiwalled Carbon Nanotubes Electrospun Fibers

Christian Narváez-Muñoz[1,2*], Camilo Zamora-Ledezma[3*], Pavel Ryzhakov[1,2], Jordi Pons-Prats[4,2], Jeevithan Elango[5], Carlos Mena[6], Freddy Navarrete[6], Víctor Morales-Flórez[7], Rafael Cano-Crespo[7], Luis Javier Segura[6,8]

[1]Escola Tècnica Superior d'Enginyers de Camins, Canals i Ports, C/Jordi Girona 1, Campus Nord UPC, Universitat Politècnica de Catalunya—Barcelonatech (UPC), 08034 Barcelona, Spain. christian.narvaez@upc.edu (C. N.-M.), pryzhakov@cimne.upc.edu (P.R.)

[2]Centre Internacional de Mètodes Numérics en Enginyeria (CIMNE), C/Gran Capitán s/n, Campus Nord UPC, 08034 Barcelona, Spain.

[3]Tissue Regeneration and Repair Group: Orthobiology, Biomaterials and Tissue Engineering, UCAM-Universidad Católica de Murcia, Campus de los Jerónimos 135, Guadalupe, 30107 Murcia, Spain. czamora9@ucam.edu (C.Z.-L.)

[4]Department of Physics, Aeronautics Division, Universitat Politècnica de Catalunya, Barcelona Tech (UPC), Edifici C3, Esteve Terrades, 5, 08860 Castelldefels, Spain. jordi.pons-prats@upc.edu (J.P.-P.)

[5]Department of Biomaterials Engineering, Faculty of Health Sciences, UCAM-Universidad Católica San Antonio de Murcia, Guadalupe, 30107 Murcia, Spain. jelango@ucam.edu (J. E.)

[6]Universidad de las Fuerzas Armadas (ESPE), Sangolquí, Ecuador. amena@fae.mil.ec (C. M.), fnavarrete@fae.mil.ec (F.N.)

[7]Departamento de Física de la Materia Condensada, Universidad de Sevilla, Avenida Reina Mercedes, 41012 Seville, Spain. vmorales@us.es, racacres@us.es

[8]Industrial Engineering Department, University of Louisville, Louisville, Kentucky, 40292, USA. ljsegu01@louisville.edu

**Authors to whom correspondence should be addressed: christian.narvaez@upc.edu (C.N.-M.), czamora9@ucam.edu (C.Z.-L.)*

Abstract:

The development of innovative and cost-efficient engineered epoxy composite material aiming to manufacture innovative and cost-efficient materials with reduced weight and enhanced physical properties remains as a current industrial challenge. In the last decades, several routes have been explored to manufacture tailored composites through the association of adhesives, polymers, and nanomaterials. In this work we report the manufacture of glass-fiber epoxy reinforced nanocomposites (GFECs) by employing electrospun fiber (EF) as a reinforcing phase produced from polyacrylonitrile (PAN) and multiwalled carbon nanotubes (MWCNT) solutions. Optimal protocols are researched by combining Taguchi method with the morphological, structural and mechanical properties obtained by Scanning Electron Microscopy (SEM), profilometry and tensile test. It is demonstrated that GFECs fabricated using GF800 glass fiber exhibits mechanical properties enhancement with a fracture strain up to 500 MPa (around 20 % compared with the non-reinforced epoxy composite counterpart). It is also shown that GFECs fabricated using GF3M glass fiber exhibited a reduction of the roughness up to 56 %, which corresponds with a roughness improvement from N8 to N7 following the guidelines provided by the ISO 1302. These results suggest that similar nanocomposites would be suitable to be harnessed in in the aeronautics and automotive industries.

Keywords: profilometry; PAN; MWCNT; carbon nanotubes; reinforcing; mechanical properties;

1.- Introduction

The design and development of cost-efficient engineered epoxy composite materials with enhanced durability and reliability remain to date as one of the most challenging topics on Materials Science research and industrial-scale [1,2]. As far as the aeronautics and automotive industries are concerned, numerous efforts have been paid over the last decades to the development of advanced epoxy composite materials with reduced weight and enhanced physical properties aiming to decrease energy consumption. Indeed, common composite materials applied in aeronautics include, but are not limited to, resin-based reinforced materials such as carbon, ceramic and glass fibers for manufacturing both structural and utility components such as propellers, wing assemblies and rotor blades among others. Ideal composites must exhibit low density, high mechanical strength, toughness, resistance to fatigue/corrosion and enough flexibility to manufacture complex shapes. All these physical parameters pursue to improve the efficiency of the engine and reduce the energy wasting [1,3,4]. It is worth mentioning that the market of aerospace composites reached more than 40 billion USD in 2020 with expected growth at a Compound Annual Growth Rate (CAGR) of about 6 % during the next four years (2022-2026) [5]. Thus, the development of cost-efficient epoxy composites at an industrial scale would remain a very appealing and interesting research trend due to their potential economic, environmental and sustainability impact.

Current preparation methods of epoxy composite materials manufacture routes are mainly founded on adhesive bonding or interlayer toughening [6–9]. Both approaches allow homogeneous incorporation of sub-phases within the interlaminar region aiming to create a uniform stress distribution. It is worth nothing that both manufactures routes exhibit intrinsically limitations, advantage and disadvantages. Indeed, these methodologies have been largely used at an industrial scale instead of those involving the use of bolts, nuts and screws that would add unnecessary weight and provide high-stress concentration points, promoting a more fragile structure. The latter would represent the main advantages. Epoxy reinforcement is usually achieved through the improvement of both the transverse crack and the delamination resistance. The typical failures originate at the micro/nanoscale and then, the failure is propagated throughout the whole macroscopic structure [6,9–11]. In the last decades, several routes have been explored to overcome these shortcomings by manufacturing tailored composites through the association of adhesives, polymers, and nanomaterials [12–14]. The

inclusion of the latter nanostructures would serve to significantly improve the reduction of the nano/micro fractures and their subsequent propagation [1,3,15,16].

As widely reported in the literature, the appearance of reinforced epoxy nanocomposites has attracted more interest in the past, due to the great improvement of mechanical properties and toughness that such materials would achieve by including nanomaterials as one of their constituents [17]. An interesting approach explored to manufacture the epoxy nanocomposites via interlayer toughening consisted of using non-woven nano/microfiber as a reinforcing phase produced via electrospinning [4,18,19]. These fibers exhibit both a high surface area/volume ratio and enhanced mechanical properties. The electrospun fiber has been widely used as mechanical reinforcement in fiber-reinforced polymer matrix composites (FRPCs), providing significant fracture toughness improvement [17]. The electrospinning technique allows fabricating of tailored particles and fibers from a weakly-viscoelastic fluid with a specific dielectric constant. The particles/fibers are produced due to the interaction of the aforementioned fluid flowing and a strong electric field. The resulting material's performance, properties and structures will be modulated by changing the physicochemical features of the viscoelastic precursor solution, the experimental variables (such as the intensity of the electric field, flow speed, etc.) and the environmental conditions including temperature and humidity [20–23]. In this context, Bilge *et al.* fabricated carbon-epoxy composite laminates incorporated poly(styrene-co-glycidal methacrylate) P(St-co-GMA) nanofibers by crosslinking with phthalic anhydride (PA) as a crosslinker and tributylamine (TBA) as an initiator, and demonstrated up to 39 % improvement in tensile strength and elastic modulus compared with the control carbon-epoxy-composites [19]. They also showed that the presence of the P(St-co-GMA)/TBA-PA nanofibers could positively impact the resin morphology, promoting a hierarchical mechanical reinforcement against crack propagation [19]. The group of Wang *et al.* also reported very recently the fabrication of custom made glass fiber/epoxy composites by incorporating bioinspired montmorillonite–carbon nanotube/epoxy interface layer around the fiber with customizable mechanical properties [6]. Similarly, Neisiany *et al.* reported the fabrication and characterization of carbon-epoxy composite laminate using electrospun core-shell nanofibers. They fabricated two types of core-shell fiber, using styrene–acrylonitrile (SAN) to produce the outer shell and either epoxy resin or an amine-based curing agent as the inner core. They incorporated the core-shell electrospun fiber within the resin in the interlaminar region, which was surrounded by a unidirectional carbon fiber layer. The incorporation of such core-shell fibers did not influence the mechanical properties of the

laminated composites overall. Indeed, it was claimed that these materials exhibited self-healing capability, and they were able to resist up to three cycles [2].

The surface characteristics and physical interaction of the nanofibers used as reinforcing phase play a crucial role in epoxy composites. In this regard, Liao *et al.* reported the fabrication of epoxy-laminated composites employing electrospun ultra-fine fibers produced from cellulose acetate (CA), polyurethane (PU), and a mixture of CA/PU polymers in order to assess the influence of the surface chemistry and roughness on the final composite performance [24]. According to their findings, the CA and CA/PU fibers exhibited a rough surface while PU a rough surface. In addition, the presence of hydroxyl groups on the surface of the CA fibers was reported. They concluded that the rough surface and hydroxyl group present in the CA fibers promoted significant improvement of the CA/epoxy adhesion, and thus huge enhancement was observed in their mechanical properties. In contrast, PU and CA/PU fibers embedded into the PU/epoxy and CAPU/epoxy composites showed poor interfacial adhesion and thus mediocre reinforcing activity [24]. In the same way, Schoenmaker *et al.* reported the fabrication and characterization of glass fibre/epoxy composite reinforced with electrospun nanofibers produced from polyamide 6 (PA) solutions. They fabricated two different sets of samples, one set consisted of fibre/epoxy nanocomposites with the PA fiber incorporated within the interlayer and the other set of samples consisted of PA electrospun fibers fabricated directly on the glass/fiber. According to their findings, they demonstrated an overall anisotropic dependence of the stress at failure. Besides, they also showed that the incorporation of electrospun nanofibers prevented the composite delamination [25]. Likewise, Kausar *et al.* reported the fabrication of Aramid-reinforced epoxy nanocomposites via a solvent casting process. They used an amine-terminated polyamide (PA) as a polymer precursor as well as functionalized and non-functionalized multi-walled carbon nanotubes (MWCNT) as additives at different content from 1 to 5 wt.%. Interestingly, they reported a higher toughness value in composites fabricated with COOH-functionalized MWCNT than the non-functionalized counterpart, which was due to the strong interaction between the OH groups present on the MWCNT surface and the amide-terminated polymeric matrix [26]. The final performance of epoxy composites will be also influenced by the methods of preparations as highlighted. In this regard, Rasheed et al. reported the influence of methods of preparation and the use of multiwalled carbon nanotube as reinforcement in Polyaniline/c-Si Heterojunction composites [9]. Another interesting work demonstrated the feasibility of producing reinforced fiber/epoxy composite laminates by using either basalt fibers, or electrospun fibers fabricated from

polyurethane (PU) and PU/carbon nanotube (CNTs) solutions [27]. They showed that the tensile and flexural properties of the reinforced fiber/epoxy composite laminate improved when PU/CNTs electrospun fibers were used as reinforcing phase, if compared with the basalt fiber-epoxy (BFEP) composite counterpart. Indeed, the composite mechanical properties improved overall as the content of CNTs increased from 1 to 5 wt.%. The incorporation of PU electrospun nanofibers into the laminate composite promoted a denser structure, with enhanced adherence. These results suggest that not only the mechanical properties of the fibers play a crucial role, but other factors such as adherence, distribution, density, and morphology would also dramatically influence the final epoxy composite performance [27].

All these aforementioned works showed the role of adding fibers as a reinforcing phase in epoxy composites and their potential applications, not only to improve the mechanical properties, but also the surface and inner morphological properties. In this regard, a large number of studies focused on the development of epoxy-based nanocomposites with enhanced fracture resistance can be readily retrieved in the literature. The majority of these works are dedicated to the mechanical reinforcement mechanism as a function of the composite thickness, diameter, and type of polymer. However, few studies have focused on exploring their simultaneous mechanical properties and surface roughness improvements, which would enormously influence their potential intended application [2–4,28]. In this work, we report the improvement of glass-fiber epoxy-based nanocomposites via interlayer toughening by employing electrospun fiber mats as a reinforcing phase. Nano/microfiber mats are fabricated from Polyacrylonitrile (PAN) solutions and their association with multi-walled carbon nanotubes (MWCNTs). Electrospun fibers are incorporated into the epoxy composites through a non-woven process. The Taguchi method is employed to minimize the number of samples to be evaluated. We then assess the morphological, structural and mechanical properties by Scanning Electron Microscopy (SEM), profilometry and tensile tests. We finally provide a phase diagram to illustrate the region where homogeneous PAN nano/microfibers mats can be manufactured.

2.- Materials and Methods

2.1.- Materials

Polyacrylonitrile (PAN) K150 was acquired from LookChem (Shanghai, China). Dimethylformamide (DMF) (purity 99.5 %, density 0.945 gm/L, molecular weight 73.09 g/mol) was purchased from Fisher Scientific (Cali, Colombia). OH-functionalized multi-

walled carbon nanotubes (MWCNTs) were purchased from NANOAMOR(Nanostructured & Amorphous Materials, Inc. Texas, TX, USA) with purity > 95 %, average length L = 2.5 μm, inner diameter d_{inner} = 4 ± 1 nm, outer diameter d_{out} = 11.5 ± 3.5 nm, specific surface area A > 233 m^2/g, bulk density ρ_{bulk} approx. 0.39 ± 0.03 g/cm^3. The epoxy composite material was manufactured using Aeropoxy Laminating Epoxy kit PR2032/PH3660 from PTM&W Industries, Inc. Such laminating resin epoxy possesses adequate viscosity and special additives to promote chemical adhesion. It was specially conceived for structural composites applications. When combined with fiber-like structures such as glass-fiber or aramid/carbon fibers, it provides excellent wet-out and satisfies the recommended Rutan Aircraft Factory (RAF) guidelines for its use in the aeronautics sector. Finally, different commercially available sources of glass-fiber with rapid penetration, saturation, and high laminate strength properties were acquired: i.- glass-fiber woven roving (GFWR) "600", labeled as GF600, with 0.6 mm of thickness and superficial density of 600 ± 30 g/cm^2; ii.- glass-fiber woven roving (GFWR) "800", labeled GF800, with 0.8 mm of thickness and superficial density of 816 ± 41 g/cm^2 and iii.- glass-fiber cloth "3M 499", labeled GF3M, with 0.2 mm of thickness.

2.2.- Methods

2.2.1.- Study design: electrospun fiber-mats optimization

The manufacture of electrospun fibers and their properties are largely influenced by: operating parameters, physico-chemical properties of the polymer-solution precursor, and environmental conditions, as was pointed out in [23]. Therefore, finding optimal scenarios with good quality fibers are often expensive and time-consuming. For this purpose, one of the main goals of the present study consists of providing an optimal set of parameter combinations for the manufacture of tailored electrospun fiber mats to be used as reinforcing phases in glass-fiber epoxy composites. In particular, we have deployed the Taguchi method (TM), which provides a systematic approach for optimizing the processing parameters, hence improving the deposited fibers. This methodology allows to readily identify the main factors that influence the composites manufacturing, which is usually time-consuming and negatively impacts the cost-effectiveness of the process [29–31]. Thus, we can significantly reduce the number of experiments by choosing an adequate orthogonal array to find optimal electrospinning parameters. To adequately choose the orthogonal array, it is necessary to appropriately identify the most influential electrospinning parameters and operating ranges (see ***Table 1***). Therefore, the main goal of this study is to find the best parameter combinations to deliver high quality fibers, namely, fine and consistent fiber diameters with enhanced mechanical properties. Then,

we have investigated three control factors: i.- tip-to-collector distance (cm), ii.- flow rate (ml/h) and iii.- PAN-polymer concentration in solution (wt.%). Also, four levels were identified, as displayed in ***Table 1.*** Subsequently, an orthogonal array of 16 runs was defined. Note that "larger is better" (LB) consideration was also established.

Table 1. Control factors and parametric levels employed for the study design according to Taguchi's design of experiments (DOE).

Control Factors	*Level 1*	*Level 2*	*Level 3*	*Level 4*
distance (cm)	15.0	16.5	18.0	20.0
flow rate (ml/h)	0.5	1.0	1.5	2.0
content (wt.%)	6.0	8.0	10.0	12.0

2.2.2.- Electrospun fiber-mats (EFMs) fabrication

To produce fiber mats, polymer solution with the adequate dielectric constant and viscoelastic properties were fabricated as follow:

2.2.2.1.- Conductive solution preparation

Following the outcome of Taguchi methods, a set of polyacrylonitrile (PAN) solutions with different contents (6, 8, 10, and 12 wt.%) were prepared using dimethylformamide (DMF) as solvent. These solutions are used as starting materials to produce fiber mats. Typically, 20 ml of DMF was poured into a 50 ml flask, then a first small amount of PAN was added to avoid polymer agglomerations. Only after the preceding part was completely dissolved, the rest of the required quantity of polymer was added until a homogeneous whitish solution was obtained. All the PAN/DMF solutions were prepared at room temperature and homogenized by a magnetic stirring bar and a magnetic stirrer at a constant velocity of 400 rpm for 3 h. In order to avoid undesired solvent evaporation, we kept the former mixture sealed during the stirring.

Similarly, the carbon nanotubes/polymer mixtures were fabricated as follows. First, a homogenous PAN/DMF solution containing the adequate content of the polymer was prepared following the procedure aforementioned[23,32]. According to the TM, the optimal content of the polymer was set at 12 wt.% and therefore all the PAN/MWCNTs fibers were prepared by keeping this concentration constant. Then, different amounts of MWCNTs powder were added

directly to the PAN/DMF solution: 0.02, 0.05, 0.1, 0.2 and 0.4 wt.%. As widely known from the literature, carbon nanotubes are by nature hydrophobic and they are not spontaneously soluble in the majority of the solvents [33,34]. For this reason, we have chosen COOH-functionalized MWCNTs which are much easier to disperse in different media. The former PAN/MWCNTs/DMF mixture was subsequently homogenized for 60 min until a dark and homogeneous blend was obtained by tip sonication (Fisherbrand model 505 sonic dismembrator) equipped with a 13 mm tip operating at 20 watts, which delivered pulses of 0.5 s separated by 1 s rest intervals. It is important to mention that samples were kept in an ice bath during sonication to avoid undesired sample overheating that would cause polymer desorption and nanotubes re-aggregation.

2.2.2.2.- Electrospun fiber mats

Electrospun fiber mats (EFMs) were obtained from the PAN/DMF and PAN/MWCNTs/DMF mixtures aforementioned. All the fibers were fabricated using an EHD-TECH Lab-Research Electrospinning Machine. The electrospray setup consisted of a high-voltage source, a syringe pump, a spray tip with a 0.4 mm inner diameter and a horizontal collector plate. It is important to mention that commonly EFMs are produced on aluminum foil, which often impedes the process of detachment of the fiber-film from it. In consequence, for either SEM observation and tensile tests, the present EFMs were spun on parchment paper. The previously depicted conductive mixture solutions were poured into a 10 ml plastic syringe and then vaporized vertically and collected on parchment paper. The optimal parameters used for our samples (16 runs) were obtained from TM and they are summarized in ***Table 2.*** Standard tip-to-collector distance and flow rate varied from 15 cm to 20 cm and from 0.5 ml/h to 2.0 ml/h, respectively. The onset voltage was obtained following the recommendation proposed in [23], it was adjusted slightly for each sample in order to reach a stable Taylor cone and varies from 11 to 20 kV. The fiber mats were obtained after 3 h. All electrospun fibers were produced at room temperature and relative humidity of 50 %. Three replicates were performed and the average values of the fiber diameters were obtained from the corresponding histograms with at least 100 measures per sample. The fiber diameter average was calculated by using ANOVA. Following the LB method, we choose the fiber-mat with optimized parameters to be subsequently used as the reinforcing phase. ***Figure 1*** shows a schematization of the fabrication process for the electrospun fiber-mats (EFMs).

Table 2. List of the total 16 experiments runs according to the study design following Taguchi's methodology. Polymer content (wt.%), flow rate (ml/h), tip-to-collector distance (cm), voltage in (kV) and average diameter (d_f) of the fibers are listed.

sample	PAN wt.%	Q (ml/h)	*d* (cm)	*V* (*kV*)	d_f (*nm*)
1	6	1.5	18.0	20.1	0.000
2	6	2.0	20.0	19.7	0.236
3	6	0.5	15.0	12.4	0.117
4	6	1.0	16.5	18.7	0.130
5	8	2.0	18.0	20.7	0.236
6	8	1.0	15.0	12.4	0.205
7	8	1.5	20.0	17.2	0.233
8	8	0.5	16.5	11.5	0.267
9	10	1.0	20.0	15.0	0.411
10	10	0.5	18.0	11.1	0.382
11	10	2.0	16.5	20.2	0.388
12	10	1.5	15.0	16.2	0.381
13	12	0.5	20.0	11.4	0.461
14	12	1.5	16.5	15.0	0.453
15	12	2.0	15.0	15.5	0.462
16	12	1.0	18.0	15.3	0.371

2.2.3.- Reinforced glass-fiber epoxy composites (GFECs) fabrication

In order to fabricate the reinforced glass-fiber epoxy composites (GFECs) by using electrospun fibers mats (EFMs) as reinforcement phase, the following procedure was followed. The fibers were directly spun over the specific glass-fiber matrix. Typically, squares of 25 cm^2 of area were placed onto the horizontal collector plate. The PAN and MWCNTs content in the precursor conductive mixtures were fixed at 12 wt.% and 0.05 wt.%, respectively. Electrospun fibers were produced by using optimal tip-to-collector distance and flow rate of 18 cm and 1 ml/h, respectively. These parameters were chosen following TMs.

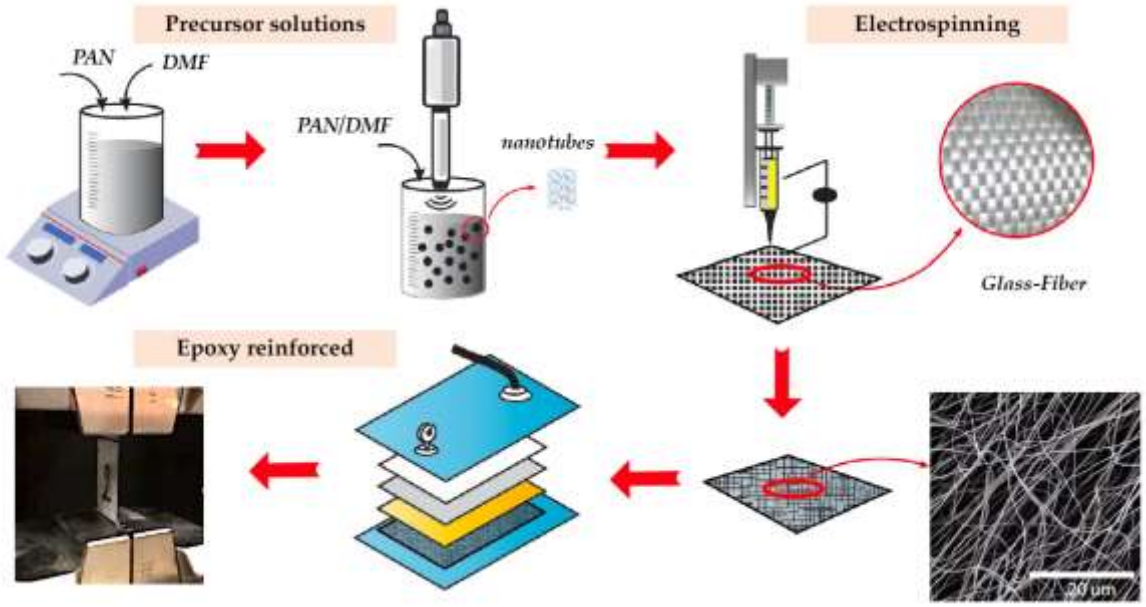

Figure 1. Schematization of the fabrication process for the electrospun fiber-mats (EFMs) and their corresponding GFECs.

Finally, the epoxy composites were prepared by pouring the resin in a ratio of 60:40 *i.e.* 60 % of resin and 40 % of fibers as recommended by the manufacturer. The standard procedure involves the use of 2 drops of hardener per 10 g of epoxy resin. Typically, a nylon vacuum bagging film was placed at the base of the mold. Then, the FGs were placed on top of it and the resin was spread carefully with a plastic spatula until the whole FGs exhibited a dark color indicating its complete impregnation with the resin. Peel Ply and Breather/Bleeder cloths were subsequently placed on the top of the resin in order to remove excess resin and to promote a uniform vacuum formation on the whole sample. Finally, the reinforced glass-fiber epoxy was cured in a vacuum oven at 80 ^{o}C for 1 hour. In ***Figure 2***, it is shows a schematization of the different layers present in the final reinforced composite. Hence, a set of reinforced and non-reinforced samples varying the glass-fibers source were prepared. It is important to mention that reinforced GFECs samples with PAN/MWCNTs electrospun fibers were fabricated by placing the EFMs facing the bottom nylon film (i.e. located between the Glass-Fiber reinforced and the bottom nylon layer see ***Figure 2***). The set of obtained samples involves 6 different types of epoxy-composites, which were labeled as CX or CXR, where X (600, 800 or 3M) stands for the type of GF, and the R is used for composites with the reinforcing EFM.

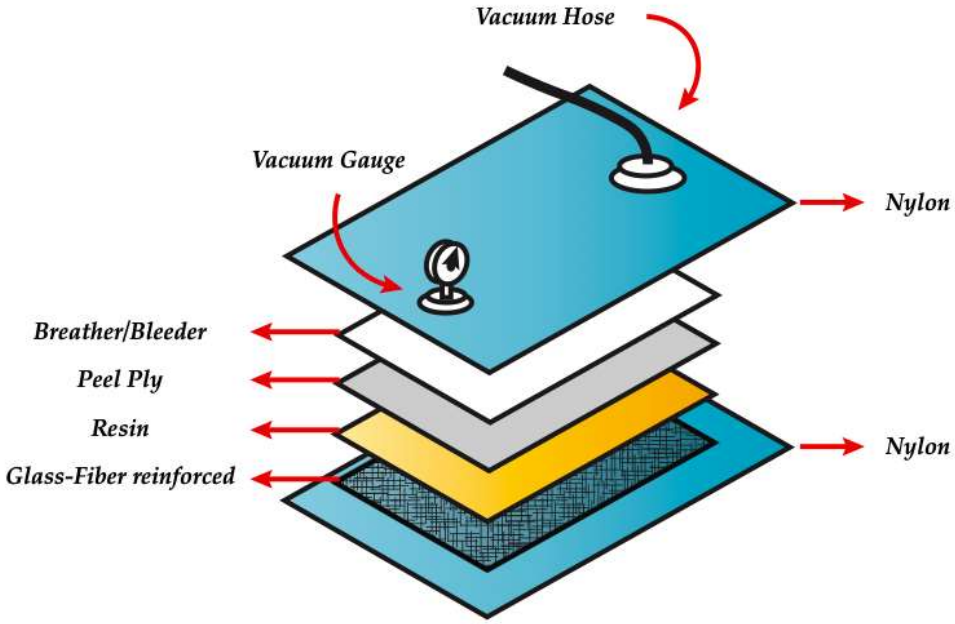

Figure 2. Schematic representation of the multi-layered glass-fiber epoxy composites (GFECs) material

2.4.- Tensile Tests

The mechanical properties of the electrospun fiber-mats (EFMs) and their corresponding reinforced glass-fiber epoxy composites (GFECs) were assessed through tensile tests performed in a ZWICK ROELL machine. Either the electrospun PAN and PAN/MWCNTs-fiber-mats and their corresponding reinforced glass-fiber epoxy composites (GFECs) were conducted following the guidelines provided by the American Society for Testing and Materials (ASTM) ASTM D3039/D3039M [35]. Due to the marked macroscopic differences between electrospun fiber mats and their corresponding epoxy-composites, two different loads were employed for tensile tests depending on the set of samples researched. Thus, the load cell changed from 1.02×10^{-3} to 5 tons for the EFMs and GFECs, respectively. Tensile specimens with adequate geometry were obtained by using clamps that can be held in the universal testing machine. Sample dimensions were measured in triplicate by using a micrometer with 10^{-3} mm of appreciation.

2.5.- Scanning Electron Microscopy (SEM)

SEM observations of the EF mats were carried out by a JEOL JSM-7001F. Samples were coated with a 20 nm thick conductive gold layer (99.99 % purity) using a sputtering evaporator. The operation voltage was 10 kV. The distribution and average fiber diameter sizes were

computed using the ImageJ software. In order to carry out an adequate statistical analysis at least 100 fibers were measured over the entire sample. Moreover, In-plane and cross section surfaces of the GFECs were observed by a FEI TENEO in the mode of secondary electrons (SE) and backscattered electrons (BSE) with an operator voltage of 5 kV. Cross section surfaces were prepared by cutting the samples with a diamond cutting saw at high speed in order to check the microstructure. It was also necessary to coat the samples with a 10 nm platinum layer (99.99 % purity) using a LEICA EM ACE600 sputtering evaporator.

2.6.- Profilometry

The roughness of all the GFECs were measured with an 3D optical-confocal microscope-interferometer (*Sensofar* S-NEOX) and the *SensoMaps* software. The surfaces were photographed with an optical microscope (model Leica DMRE, *Leica Microsystems GmbH*, Germany). A magnification of 50× was employed with a gaussian filter of 80 μm. The value of this magnitude was estimated through the value of the linear average arithmetic roughness, R_a. This magnitude is defined as the arithmetic mean of the absolute value of the height *y(x)* from the average height of the profile:

$$R_a = \frac{1}{l}\int_0^l |y(x)|\, dx \qquad \text{Eq. (1)}$$

Two regions were explored per sample, and ten values of R_a corresponding to ten parallel lines (profiles) and another ten values from parallel lines perpendicular to the first ones were obtained on each region. In summary, 20 values of the roughness were acquired on each region and 40 values on each sample. An statistical analysis was performed to obtain the average values and the corresponding standard deviations. 3D topographies were taken with the help of the profilometer analysis software *SensoMaps* and with the optical microscope mentioned previously.

3.- **Results and discussion**

Morphological, structural and mechanical properties were discussed with Scanning Electron Microscopy (SEM), profilometry and tensile tests as the most appropriate protocols with Taguchi method to optimize the number of samples to be evaluated for the electrospinning process, and also to establish a phase diagram with optimal parameters for the fabrication of homogeneous PAN/MWCNTs fibers composites.

3.1.- Scanning Electron Microscopy (SEM) analysis of the EF mats

The structural and morphological features of the PAN-electrospun fibers mats (PAN-EFMs) were researched by scanning electron microscope (SEM). In ***Figure 3 (a-d),*** we showed representative microscopies of PAN-EFMs produced following different experimental conditions (flow rate, tip-to-collector distance and voltage). It was demonstrated that sample morphology varied from the bead, beaded-fibers and fibers accordingly. For instance, samples fabricated from PAN 6 wt.% at 1.5 ml/h, 18 cm and 20 kV formed solely beaded particles, and thus we were unable to measure any fiber diameter. For the rest of the samples examined, a clear trend was observed regardless of the flow rate, tip-to-collector distance or voltage. Thus, as the PAN content increases, the number of beads decreased significantly (up to almost totally disappear) and the diameter of the fiber was increased accordingly from 0.1 up to 0.5 micrometers as illustrated in ***Figure 3 (e)*** in which we have plotted the average fiber diameter obtained from their corresponding histograms. These characteristic features are in total agreement with the literature, and are often attributed to the jet instability during electrospinning [36–39].

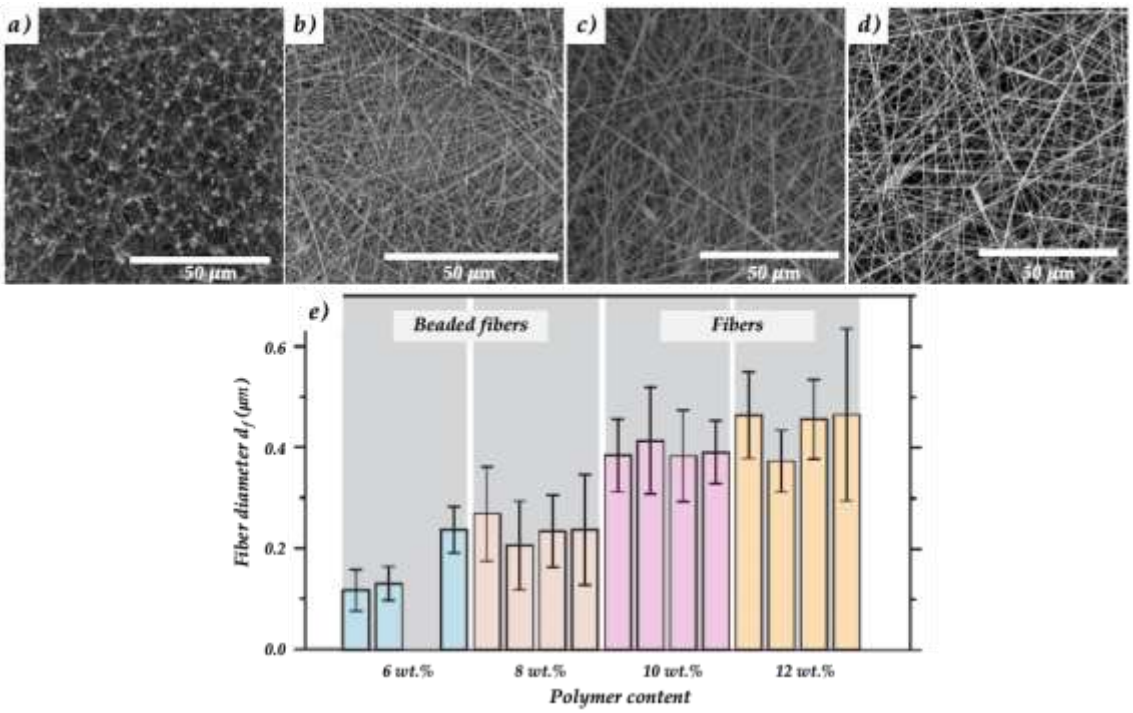

Figure 3. Representative SEM images for PAN-fibers fabricated under different operational parameters (flow rate, tip-to-collector distance and voltage) and polymer content according to Taguchi method (a-d). The average fiber diameters obtained from their corresponding histograms are plotted in (e). Each column informs about the average value and the standard deviation obtained from one SEM image.

The latter effect has been extensively discussed in the literature, and commonly appears when the polymeric precursor solution did not have the adequate elasticity to stretch its polymer chains by the electric force [21,23,34]. Additionally, we also observed slight differences in the fiber morphologies/structures and fiber diameters when the PAN wt.% content is kept constant, but we changed the operational parameters. According to these results, the polymer concentration stands as the most significant parameter to control the fiber size distribution, while the second most significant parameter is the flow rate according to the control factors and parametric levels used through Taguchi's design of experiments (DOE). For its part, in ***Figure 4*** the trend diagram of each parameter on the fiber diameter, obtained from Taguchi's results in a mean of signal-to-noise response is shown. Open circles denote optimal parameters for the production of single fiber morphology from "larger is better" (LB).

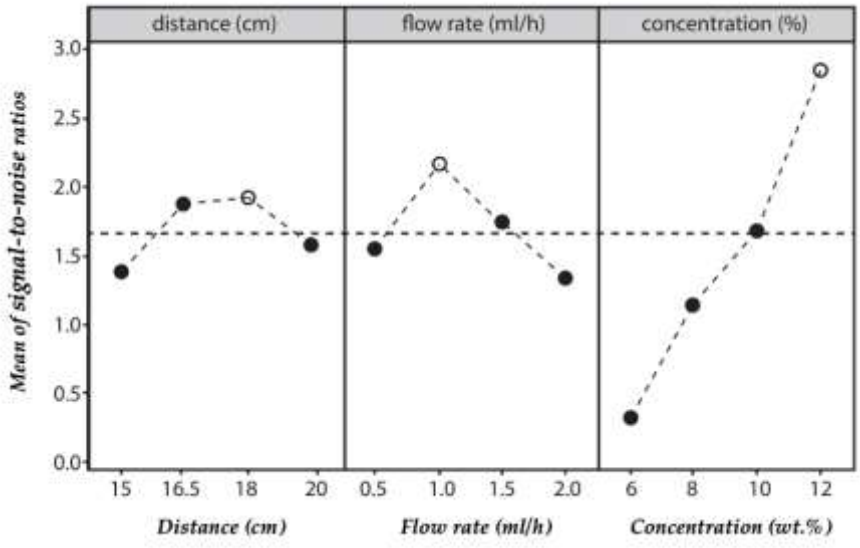

Figure 4. The trend diagram of each parameter on the fiber diameter, obtained from Taguchi's results in a mean of signal-to-noise response. Open circles denote optimal parameters for single fiber morphology from "larger is better" (LB).

The combination of the data obtained from SEM, histograms and the trend diagram allowed us to build the diagram of stability for PAN fiber mats (see ***Figure 5***). In this plot, we summarized the control factors used for electrospinning as a function of the electric field applied, the flow rate and the polymer content. An unequivocal stability belt (gray zone) corresponding to the region exhibiting optimal parameters to obtain fiber-mats is observed. The bounds of the belt were determined by testing each combination of control factors with its respective onset voltage. As widely known from the literature, during the electrospinning experiments, the adequate voltage is unknown, thus, the typical experimental methodology involves varying the voltage in small steps until the polymer solution at a given flow rate forms a stable cone jet mode [21,37–39]. It should be noted that there exists a strong relationship between flow rate and electric field. Indeed, the solution with 6 wt.% of polymer content exhibited an unstable jet, and was thus difficult to control with the electric field provoking solely isolated particles. On the contrary, polymer content from 8 to 12 wt.% produced different fiber and beaded-fiber morphologies by tuning the electric field and flow rate. The latter diagram results are very useful for the fabrication of fiber mats with specific morphologies, and demonstrate that such materials can be readily obtained by varying the values of flow rate and electric field around the stable zone.

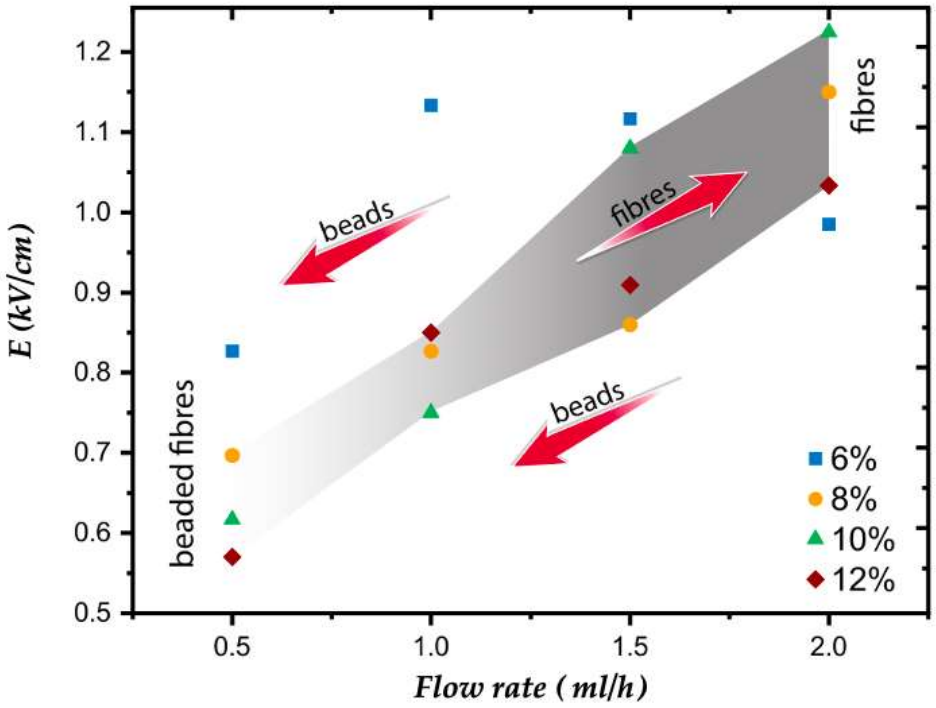

Figure 5. Diagram of stability for the control factors used for electrospinning as a function of the control factors, *i.e.* the applied electric field, the flow rate and the polymer content. Gray area denotes the stability belt, *i.e.* the region with optimal parameters to obtain fiber-mats.

3.2.- Structural and mechanical characterization of PAN-EFMs

The mechanical characterization of the electrospun fiber mats was carried out in order to assess the response of the fibers to an external force, providing their main mechanical features such as the Young's Modulus (E), the ultimate tensile strength (UTS) and fracture strain. With this aim, typical stress-strain curves were obtained for all the samples studied. ***Figure 6*** shows representative stress-strain curves of the set of fibers made from a set of polyacrylonitrile (PAN) solutions at different content (6, 8, 10, 12 wt.%). As observed in the figure, all the PAN-fiber mats researched from solutions at 6 wt.% and 8 wt.% showed a very fragile behavior with a fracture strain below 8 %, and a tensile strength inferior to 1 MPa. It's worth noting that, regardless of the fiber morphology shown in the SEM pictures (***Figure 3***), all the solutions were able to generate a fiber mat with the exception of the combination of a solution with PAN 6 wt.% at 1.5 ml/h, 18 cm and 20 kV, which formed solely beaded particles (see Fig. 5). On the contrary, PAN-EFMs fabricated at higher polymer content (10 wt.% and 12 wt.%), showed improved mechanical properties with a fracture strain up to 30 % accompanied by a tensile strength of 3 MPa, and a Young modulus ranging from 0.1 to 0.7 MPa and comparable with those reported in the literature [14,18,40,41]. ***Table 3*** summarizes the mechanical properties

for electrospun PAN-fiber-mats samples fabricated at different PAN wt.% content. It is also worth mentioning that we also observed changes in the mechanical properties depending on the operational parameters such as the flow rate and the electric field as summarized in ***Figure 7***. We also noted that in the microscopical examination of the fiber mats before and after the mechanical tests, fibers tend to align parallel to the stretching direction (see ***Figure 8*)**, as expected. This phenomenon has been widely discussed in the literature and would be another open way to confer improved mechanical properties to electrospun fiber mats by including a pre-stretching treatment when they are intended to use as a reinforcing phase [18,39,42,43]. Fiber mats with preferential orientational order morphologies are also highly appealing for biomedical and biomimetic applications, indeed, it has been shown that similar structures promote cellular migration and proliferation enhancement [44–48]. Finally, the statistical analysis showed that there was no significant difference in the fiber diameters with a value of $p > 0.05$ for all the sets of electrospun samples. All these results from the trend diagram, SEM, the diagram of stability and their corresponding mechanical properties allowed us to choose the best operational parameters to produce electrospun PAN/MWCNTs fiber mats as reinforcing phase. Thus, the optimal parameters used from now on are:vi.- tip-to-collector distance = 18 cm, ii.- flow rate = 1 ml/h and iii.- PAN content = 12 wt.%.

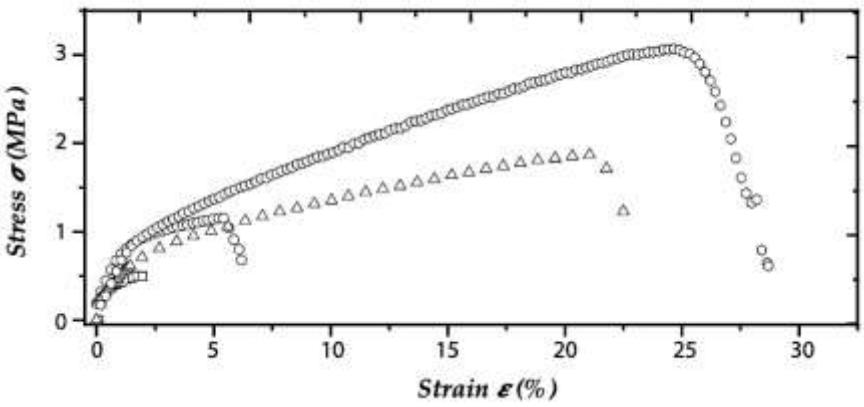

Figure 6. Stress versus strain for electrospun PAN-fiber-mats samples fabricated from PAN/DMF-solutions at different PAN content: 6 wt.%, (open squares), 8 wt.% (open circles), 10 wt.% (open triangles), 12 wt.% (open hexagons).

Table 3. Mechanical properties for electrospun PAN-fiber-mats samples fabricated at different PAN wt.% content. E denotes the Young's modulus, UTS denotes the Ultimate Tensile Strength and ε_{max} denotes the fracture strain.

PAN wt.%	*E (MPa)*	*UTS (MPa)*	ε_{max} *(%)*
6	0.16	0.50	2.15
6	0.07	0.12	2.27
8	0.35	1.03	5.49
8	0.38	1.18	8.50
8	0.25	0.70	5.89
8	0.58	1.51	8.40
10	0.13	2.00	28.00
10	0.28	1.45	28.07
10	0.45	1.26	16.63
12	0.70	2.88	31.38
12	0.20	2.40	31.86
12	0.54	3.10	27.67

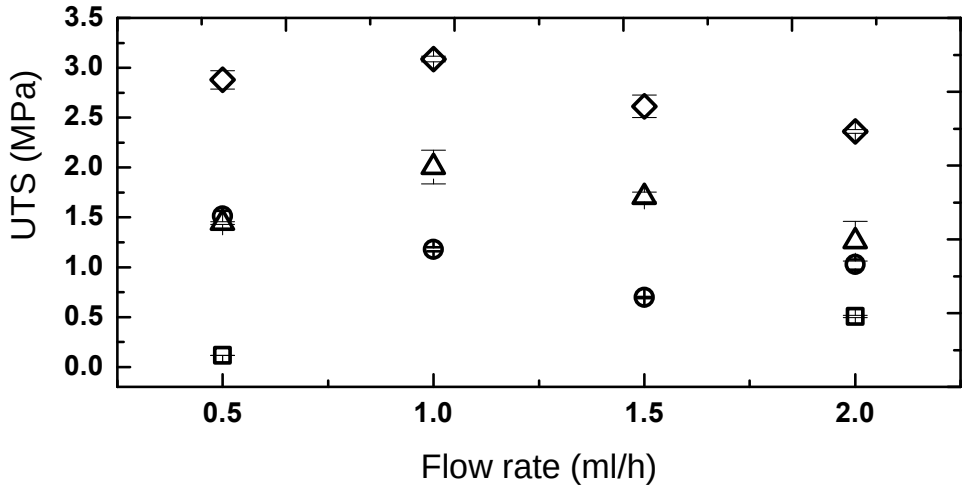

Figure 7. Ultimate Tensile Stress (UTS) computed from tensile tests carried out on PAN-fiber-mats. Electrospun mats were fabricated from PAN/DMF-solutions at different flow rates and PAN wt.% content (open squares 6 wt.%, open circles 8 wt.%, open triangles 10 wt.%, open hexagons 12 wt.%).

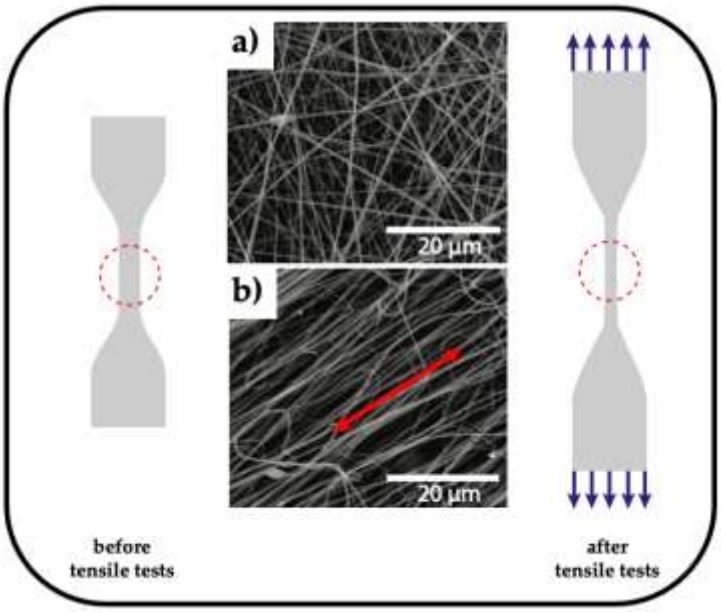

Figure 8. Schematization of fiber arrangement before and after tensile tests in PAN electrospun mats. Representative SEM micrographs for fiber mats fabricated from a PAN/DMF-solution at 12 wt.% and 1.0 ml/h of flow rate for a) before and b) after tensile tests. Red arrow in b) indicates the direction of the tensile stress. As expected, PAN-fibers tend to align preferentially throughout the stretching direction.

3.3.- Structural and mechanical characterization of PAN/MWCNT fiber mats

As detailed in the materials and methods section, the fabrication of the PAN/MWCNTs fiber mats was carried out in a two-step process. We have kept constant the tip-to-collector distance = 18 cm, the flow rate = 1 ml/h, the PAN content = 12 wt.%, and we have varied the content of nanotubes in the solution mixtures from 0.02, 0.05, 0.1, 0.2 and 0.4 wt.% respectively. We solely varied the electric field slightly in order to obtain a stable Taylor cone. The structural and morphological features of the PAN/MWCNTs-electrospun fibers mats (PAN/MWCNT-EFMs) were investigated by scanning electron microscope (SEM), and showed similar qualitative behavior to their 12 wt.% PAN-fiber-mats counterpart. *i.e.* samples typically exhibited single fiber morphology as expected. In the inset of the ***Figure 9***, a representative SEM image of the PAN/MWCNT-fiber-mat with PAN/MWCNT content of 12/0.05 wt.% respectively and average fiber diameter $d_f = 0.6 \pm 0.1$ $\boldsymbol{\mu}$m. Is it worth mentioning that all fiber mats fabricated from PAN/MWCNT/DMF solutions exhibited systematically average diameters bigger than their PAN native counterpart, induced by the presence of the carbon nanotubes. As far as their mechanical properties are concerned, in ***Figure 9*** the typical stress-strain curve for the PAN/MWCNTs fiber-mats for the set of samples containing different loads of carbon nanotubes. As observed, fiber-mats containing the lower MWCNTs loads (0.02 wt.%

and 0.05 wt.%) exhibited improved mechanical behavior when compared with the PAN native counterpart. Indeed, samples with 0.05 wt.% of MWCNTs showed a tensile strength of 4.5 MPa and a fracture strain of about 40 %, which represent almost improvements of 50 % and 33 % if compared to their native PAN at 12 wt.% counterpart. We also observed that, as the content of MWCNTs increased (beyond 0.05 wt.%), the mechanical properties of the specimen showed a non-negligible deterioration. This "saturation" phenomenon has commonly been observed in similar systems such as those based on polyvinylpyrrolidone (PVP)/CNTs electrospun fibers or even other composites reinforced with carbon nanotubes. In such a system, the worsening of the mechanical properties was attributed to a poor and non-homogenous carbon nanotube dispersion within the composites. Hence, the formation of clusters of carbon nanotubes within the matrix often tend to concentrate the stresses or even act as defects and crack initiators, provokes more fragile materials [34,49–51]. Thus, the optimal parameters used from now on are: i.- tip-to-collector distance = 18 cm, ii.- flow rate = 1 ml/h, iii.- PAN content = 12 wt.% and MWCNT content = 0.05 wt.%. ***Table 4*** summarizes the mechanical properties for electrospun PAN/MWCNT-fiber-mats samples fabricated with 12 wt.% PAN and different MWCNT wt.% content.

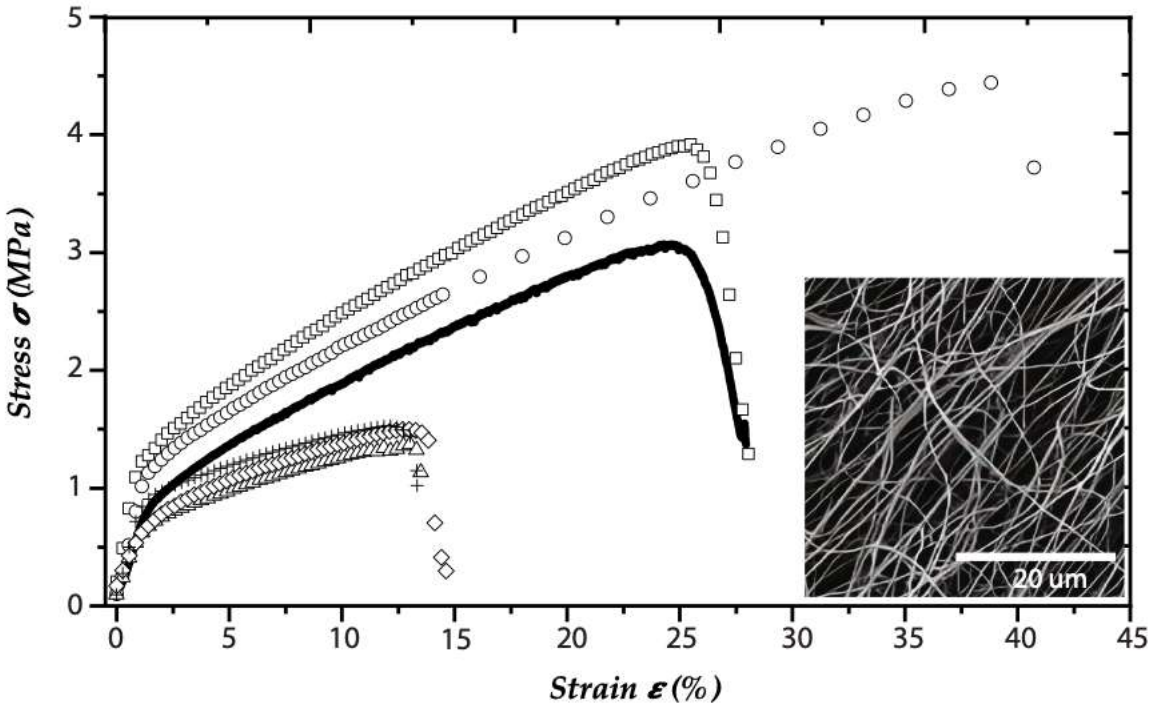

Figure 9. Stress versus strain for electrospun PAN/MWCNT-fiber-mats samples fabricated from PAN/MWCNTs/DMF-solutions with 12 wt.% PAN and 0 wt.% (continuous black solid line), 0.02 wt.% (open squares), 0.05 wt.% (open circles), 0.1 wt.% (open triangles), 0.2 wt.% (open diamonds), 0.4 wt.% (plus symbols) MWCNTs. Inset shows a representative SEM image

of the PAN/MWCNT-fiber-mat with MWCNT content of 0.05 wt.% and average fiber diameter $d_f = 0.6 \pm 0.1\ \mu$m.

Table 4. Mechanical properties for electrospun PAN/MWCNT-fiber-mats samples fabricated with 12 wt.% PAN and different MWCNT wt.% content. **E** denotes the Young's modulus, **UTS** denotes the Ultimate Tensile Strength and ε_{max} denotes the fracture strain.

MWCNT (wt.%)	*E (MPa)*	*UTS (MPa)*	ε_{max}*(%)*
0.00	0.54	3.10	27.67
0.02	1.05	3.67	31.57
0.05	0.60	3.89	37.46
0.10	0.50	1.46	12.82
0.20	0.41	1.78	18.42
0.40	0.70	1.76	11.82

3.4.- Structural and mechanical characterization of reinforced glass-fiber epoxy composites (GFECs)

As depicted in the materials and methods section, we have prepared a set of glass-fiber epoxy composites (GFECs) reinforced with Electrospun-Fiber Mats (EFMs) based on PAN/MWCNTs and using different glass-fiber sources: a) GF3M, b) GF600 and c) GF800. All the reinforced GFECs were fabricated using PAN/MWCNTs fibers as reinforcing phases with a constant content of PAN and MWCNTs of 12 wt.% and 0.05 wt.%, respectively. These EFMs exhibited the optimal combination of both structural and mechanical properties. ***Figure 10*** representative in-plane and cross-section SEM images of reinforced GFECs are shown. These images allow us to appreciate the multi-layered epoxy-composites material characteristic features. In particular, ***Figure 10-d*** shows a representative cross section SEM image of the GFECs fabricated with GF3M (namely C3MR) in which the densely packed region of glass-fiber is embedded in resin.

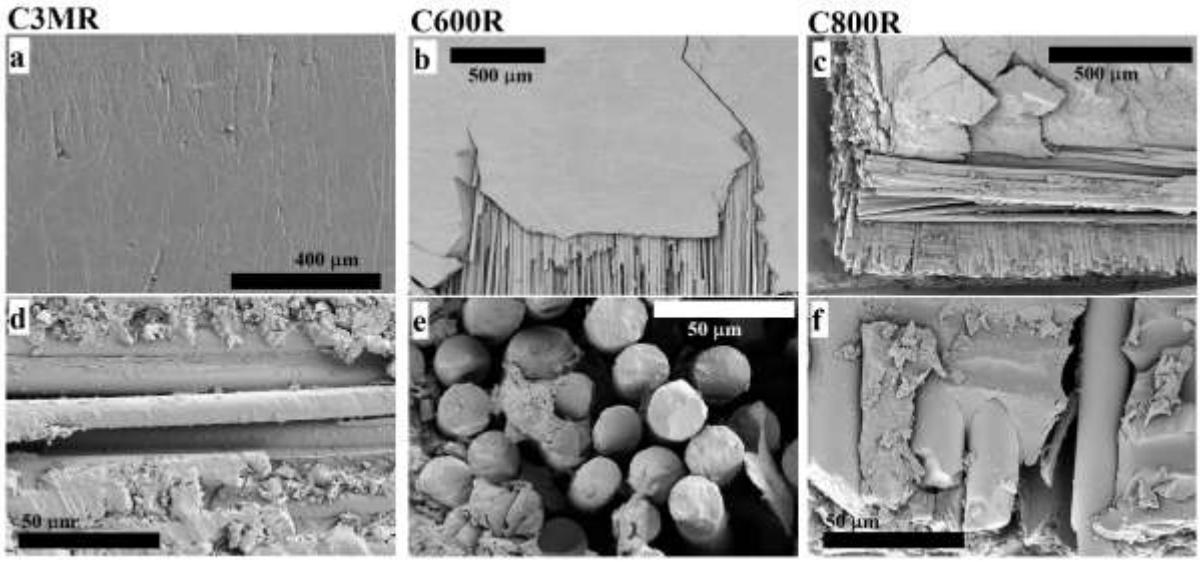

Figure 10. Representative in-plane and cross-section SEM images of reinforced glass-fiber epoxy composites with PAN/MWCNTs electrospun fibers, and employing different sources of glass-fiber: a-d) GF3M, b-e) GF600, and c-f) GF800 respectively.

For its part, **Figure 11** provides the comparison between the stress-strain curves from the composite with and without the reinforcement. In order to differentiate the native multi-layered epoxy-composites material from the reinforced one, samples are labeled as CX or CXR, where X (3M, 600 or 800) stands for the type of GF, and the R is used for composites fabricated with PAN/MWCNTs-fiber mats (EFMs) as a reinforcing phase. As observed, native GFECs without reinforcing phase showed tensile strengths ranging from 250 to 450 MPa accompanied by a very low fracture strain (below 8 % as most). The inclusion of the PAN/MWCNT electrospun fibers does not improve or deteriorate their overall mechanical properties. Similarly, the GFECs fabricated using the GF3M exhibit a tensile strength and fracture strain ranging from 250/280 MPa and 6/7 % respectively, and do not exhibit any improvement due to the addition of the reinforcement. In contrast, the GFECs fabricated using the GF800 showed an enhancement of the mechanical properties, including an increase of the fracture strain up to 500 MPa, which represents an improvement of almost 20 % compared with the non-reinforced epoxy composite counterpart.

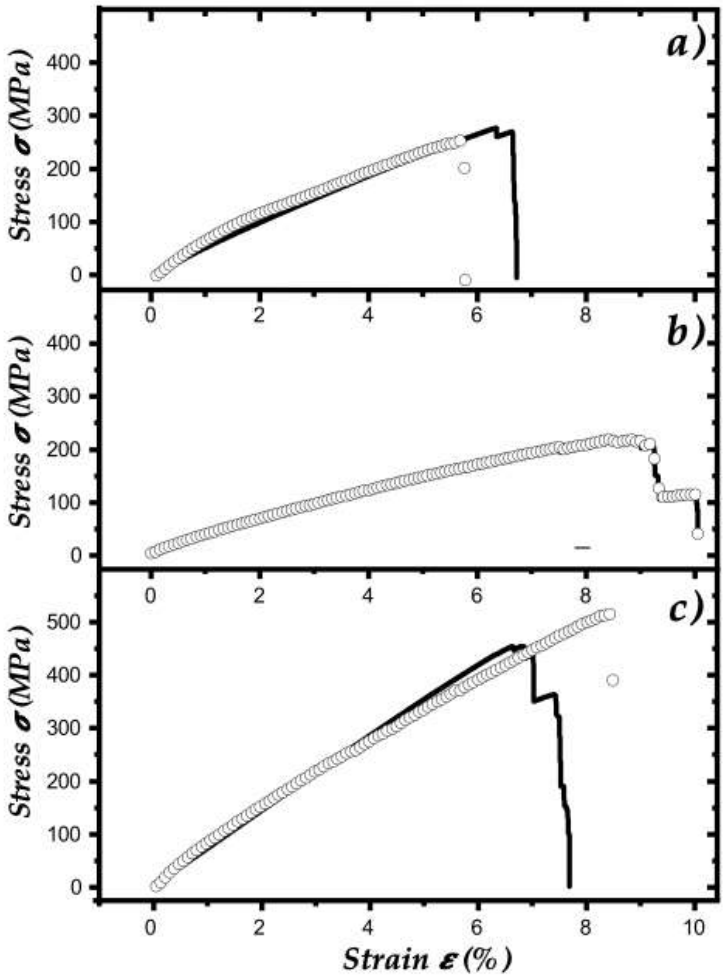

Figure 11. Stress versus strain for glass-fiber epoxy composites (GFECs) with and without PAN/MWCNTs electrospun fibers produced from PAN/MWCNTs/DMF-solutions with 12 wt.% PAN and 0.05 wt.% MWCNTs as reinforcing phase. In the picture, we have represented by open circles the GFECs with the reinforcing phase while the continuous line represents the GFECs without the reinforcing phase. Samples were fabricated by employing different sources of glass-fiber: a) GF3M, b) GF600 and c) GF800.

All these results were consistent with the literature [4,40,52]. The mechanical properties of the GFECs reinforced nanocomposites were not significant with the exception of those fabricated by employing the glass-fiber FG800.

Regarding the surface roughness of the sample series, it was demonstrated that the roughness of the final epoxy composites changed dramatically. ***Table 5*** and ***Figure 12*** show the results of roughness for all the studied materials. As observed, samples exhibited values of average roughness ranging between 15 to 35 nm. It can be appreciated that the roughness of the samples without reinforcement were systematically higher than the roughness of those samples with reinforcement (suffix R). The most significant changes were observed for samples fabricated with 3M glass-fiber reinforced with a reduction of the roughness up to 56 %, which correspond

with a roughness improvement from N8 to N7 following the guidelines provided by the ISO 1302 [53]. In ***Figure 12*** is also shown a comparative between representative 3D topographies of the surface for the samples C3M (non-reinforced) and C3MR. It is worth mentioning that such improvements of rugosity accompanied by adequate mechanical response are properties highly desired for materials to be harnessed in different sectors such as aeronautics and automotive industries [52,54,55].

Table 5. Values for the horizontal and vertical average arithmetic roughness in a line (Ra) for all the samples.

	HORIZONTAL ROUGHNESS (nm)	VERTICAL ROUGHNESS (nm)	AVERAGE ROUGHNESS (nm)
C3MR	15 ± 1	18 ± 2	16 ± 1
C3M	15 ± 1	57 ± 6	36 ± 4
C600R	14 ± 1	20 ± 3	17 ± 2
C600	24 ± 1	25 ± 3	25 ± 2
C800R	23 ± 2	21 ± 3	22 ± 2
C800	36 ± 4	14 ± 1	25 ± 2

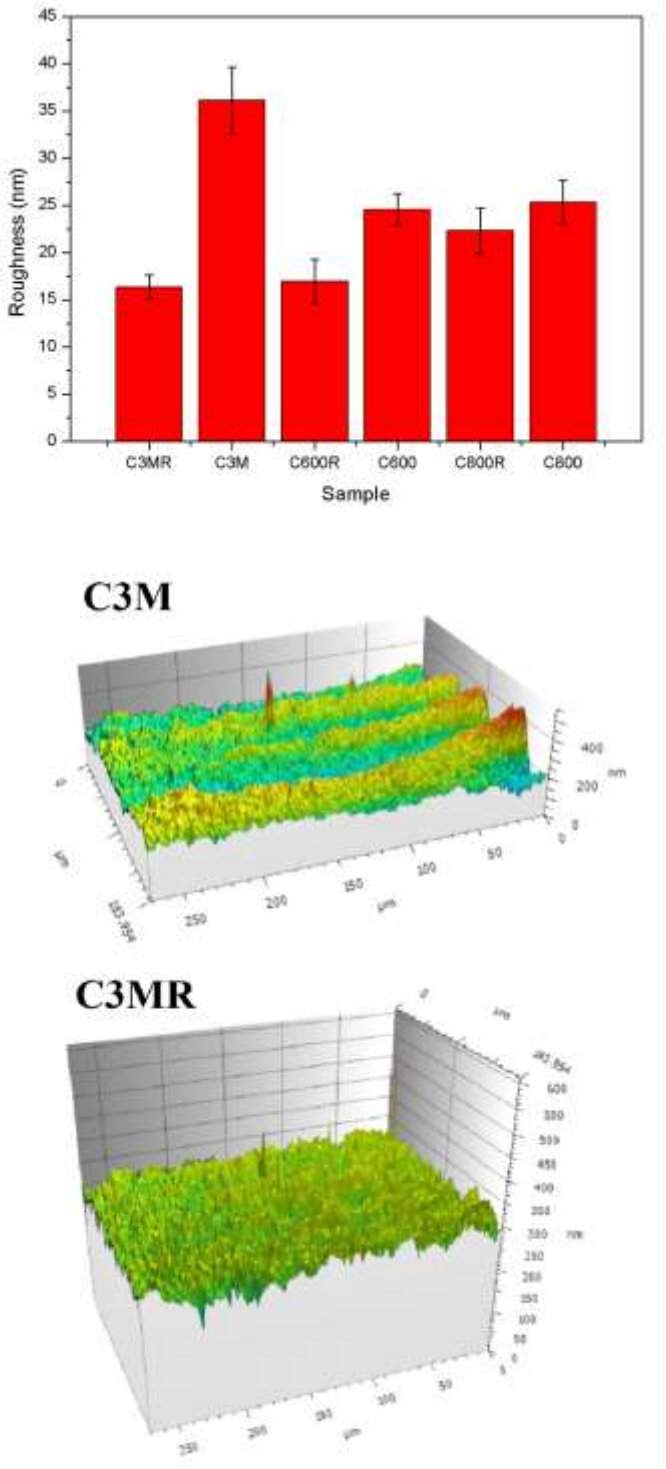

Figure 12. Top: Roughness for non-reinforced and reinforced glass-fiber epoxy composites (GFECs) using PAN/MWCNTs EFMs with 12 wt.% PAN and 0.05 wt.% MWCNTs as reinforcing phase and different sources of glass fibers: GF3M, GF600 and GF800. The sufix "R" represents the reinforced GFECs. Center and bottom: representative profilometry 3D view of the surface for the epoxy-composites C3M and C3MR.

5.- Conclusions

The fabrication of cost-efficient engineered epoxy composites materials is by far one of the major challenging topics at research and industrial scale. Industries require more performant materials with reduced weight and enhanced physical properties aiming to decrease energy consumption. Here we demonstrated for the first time that is possible to manufacture glass-fiber epoxy reinforced nanocomposites (GFECs) via interlayer toughening, by employing electrospun fibers as reinforcing phase produced from a mixture of polyacrylonitrile (PAN) and multi-walled carbon nanotubes (MWCNT) solutions. It is also established a phase diagram with optimal parameters (stability belt) for the fabrication of homogeneous PAN/MWCNTs fibers by combining Taguchi method alongside with the morphological, structural and mechanical properties obtained by Scanning Electron Microscopy (SEM), profilometry and tensile test. The latter, allowed us to optimize the number of samples to be evaluated. Composites materials GFECs fabricated using the GF800 glass fiber showed mechanical property enhancement with a fracture strain up to 500 MPa which represents an improvement around 20 % compared with the non-reinforced epoxy composite counterpart. It is also worth noting, that such GFECs nanocomposites materials exhibited an overall roughness enhancement. Indeed, we have demonstrated that the incorporation of the PAN/MWCNT electrospun fiber within the epoxy substantially decreases the roughness. Composites GFECs fabricated using GF3M glass fiber exhibited a reduction of the roughness up to 56 %, which correspond with a roughness improvement from N8 to N7 following the guidelines provided by the ISO 1302. These results suggest that similar GFECs nanocomposites would have potential applications in different sectors such as the aeronautics and automotive industries.

7.- Acronyms: Glass-Fiber (GF), reinforced glass-fiber epoxy reinforced nanocomposites (GFECs), Polyacrylonitrile (PAN), Multiwalled Carbon Nanotubes (MWCNT), Scanning Electron Microscopy (SEM), Taguchi method (TM), Compound Annual Growth Rate (CAGR), Fiber-Reinforced Polymer Matrix Composites (FRPCs), Poly(Styrene-Co-Glycidal Methacrylate) (P(St-co-GMA)), Phthalic Anhydride (PA), Tributylamine (TBA), Styrene–Acrylonitrile (SAN), Cellulose Acetate (CA), Polyurethane (PU), Multi-Walled Carbon Nanotube (MWCNTs), Larger is Better (LB), Design of Experiments (DOE), Electrospun Fiber-Mats (EFMs), Dimethylformamide (DMF), Young's modulus (***E***), Ultimate Tensile strength (***UTS***), Fracture strain ($\boldsymbol{\varepsilon_{max}}$).

8.- Supplementary Materials: Not applicable.

9.- Author Contributions: Conceptualization, C.N.M and C.Z.L.; methodology, C.N.M, C.Z.L., P.R., J.P.-P. and J.L.S.; formal analysis, C.N.M, C.Z.L., P.R., J.P.-P., J.E, and V.M.F, ; investigation, C.M., F.N. C.N.M and C.Z.L.; R.C.C and V.M.F contributed with SEM and Profilometry measurements and analysis; writing—original draft preparation, C.N.M and C.Z.L.; writing—review and editing, J.E, V.M.F., C.N.M and C.Z.L.; supervision and project administration, C.N.M and C.Z.L.; funding acquisition, C.N.M and C.Z.L.; All authors have read and agreed to the published version of the manuscript.

10.- Funding: This work was financially supported by the "Convocatoria de Ayudas a la Realización de Proyectos de Grupos de Investigación 2020-2021" of the Universidad Católica de Murcia (UCAM), Spain, Reference: PMFI-12/21. P.R., J.P-P. and C.N-M would also like to acknowledge the support of the Ministerio de Ciencia, Innovación y Universidades of Spain via the "Severo Ochoa Programme" for Centres of Excellence in R&D (reference: CEX2018-000797-S) given to the International Centre for Numerical Methods in Engineering (CIMNE). The work of C.N-M was financially supported by the "Severo Ochoa PhD Scholarship" Reference: PRE2020-096632. P.R. and J.P.-P. are Serra Hunter fellows.

11.- Conflicts of Interest: The authors declare no -conflict of interest.

12.- Acknowledgements: The profilometry images and in-plane and cross-section SEM images were acquired with the help of Consuelo Cerrillos González (CITIUS-Universidad de Sevilla).

13.- References:

[1] R. Wazalwar, M. Sahu, A.M. Raichur, Mechanical properties of aerospace epoxy composites reinforced with 2D nano-fillers: current status and road to industrialization, Nanoscale Adv. 3 (2021) 2741–2776. https://doi.org/10.1039/D1NA00050K.

[2] R.E. Neisiany, J.K.Y. Lee, S.N. Khorasani, S. Ramakrishna, Towards the development of self-healing carbon/epoxy composites with improved potential provided by efficient encapsulation of healing agents in core-shell nanofibers, Polymer Testing. 62 (2017) 79–87. https://doi.org/10.1016/j.polymertesting.2017.06.016.

[3] N. Baig, I. Kammakakam, W. Falath, Nanomaterials: a review of synthesis methods, properties, recent progress, and challenges, Mater. Adv. 2 (2021) 1821–1871. https://doi.org/10.1039/D0MA00807A.

[4] U. Montanari, D. Cocchi, T.M. Brugo, A. Pollicino, V. Taresco, M. Romero Fernandez, J.C. Moore, D. Sagnelli, F. Paradisi, A. Zucchelli, S.M. Howdle, C. Gualandi, Functionalisable Epoxy-rich Electrospun Fibres Based on Renewable Terpene for Multi-Purpose Applications, Polymers. 13 (2021) 1804. https://doi.org/10.3390/polym13111804.

[5] IMARC Group, Aerospace Composites Market: Global Industry Trends, Share, Size, Growth, Opportunity and Forecast 2021-2026, India, 2021. https://www.imarcgroup.com/aerospace-composites-market (accessed March 23, 2022).

[6] Q. Wang, S. Chen, S. Zeng, P. Chen, Y. Xu, W. Nie, Y. Zhou, Tunable mechanical properties of glass fiber/epoxy composites by incorporating bioinspired montmorillonite–carbon nanotube/epoxy interface layer around the fiber, Composites Part B: Engineering. 242 (2022) 110092. https://doi.org/10.1016/j.compositesb.2022.110092.

[7] M. Bilugali Mahadevaswamy, R. Aradhya, S. Bhattacharya, S.R. Jagannathan, Effect of hybrid carbon nanofillers at percolation on electrical and mechanical properties of glass fiber reinforced epoxy, J of Applied Polymer Sci. 139 (2022). https://doi.org/10.1002/app.52439.

[8] S. Dasari, S. Lohani, R.K. Prusty, An assessment of mechanical behavior of glass fiber/epoxy composites with secondary short carbon fiber reinforcements, J of Applied Polymer Sci. 139 (2022) 51841. https://doi.org/10.1002/app.51841.

[9] H.Kh. Rasheed, A.A. Kareem, Effect of Multiwalled Carbon Nanotube Reinforcement on the Opto-Electronic Properties of Polyaniline/c-Si Heterojunction, Journal of Optical Communications. 42 (2021) 25–29. https://doi.org/10.1515/joc-2018-0024.

[10] A.A. Kareem, Preparation and electrical properties of polyimide/carbon nanotubes composites, Materials Science-Poland. 35 (2017) 755–759. https://doi.org/10.1515/msp-2017-0096.

[11] A.A. Kareem, H.Kh. Rasheed, Electrical and thermal characteristics of MWCNTs modified carbon fiber/epoxy composite films, Materials Science-Poland. 37 (2019) 622–627. https://doi.org/10.2478/msp-2019-0081.

[12] N. Domun, H. Hadavinia, T. Zhang, T. Sainsbury, G.H. Liaghat, S. Vahid, Improving the fracture toughness and the strength of epoxy using nanomaterials – a review of the current status, Nanoscale. 7 (2015) 10294–10329. https://doi.org/10.1039/C5NR01354B.

[13] S. Liu, V.S. Chevali, Z. Xu, D. Hui, H. Wang, A review of extending performance of epoxy resins using carbon nanomaterials, Composites Part B: Engineering. 136 (2018) 197–214. https://doi.org/10.1016/j.compositesb.2017.08.020.

[14] G. Duan, S. Liu, H. Hou, Synthesis of polyacrylonitrile and mechanical properties of its electrospun nanofibers, E-Polymers. 18 (2018) 569–573. https://doi.org/10.1515/epoly-2018-0158.

[15] L.A. Kolahalam, I.V. Kasi Viswanath, B.S. Diwakar, B. Govindh, V. Reddy, Y.L.N. Murthy, Review on nanomaterials: Synthesis and applications, Materials Today: Proceedings. 18 (2019) 2182–2190. https://doi.org/10.1016/j.matpr.2019.07.371.

[16] J.R. Lead, G.E. Batley, P.J.J. Alvarez, M.-N. Croteau, R.D. Handy, M.J. McLaughlin, J.D. Judy, K. Schirmer, Nanomaterials in the environment: Behavior, fate, bioavailability, and effects-An updated review: Nanomaterials in the environment, Environ Toxicol Chem. 37 (2018) 2029–2063. https://doi.org/10.1002/etc.4147.
[17] U.A. Shakil, S.B.A. Hassan, M.Y. Yahya, S. Nauman, Mechanical properties of electrospun nanofiber reinforced/interleaved epoxy matrix composites—A review, Polymer Composites. 41 (2020) 2288–2315. https://doi.org/10.1002/pc.25539.
[18] X. Yang, J. Wang, H. Guo, L. Liu, W. Xu, G. Duan, Structural design toward functional materials by electrospinning: A review, E-Polymers. 20 (2020) 682–712. https://doi.org/10.1515/epoly-2020-0068.
[19] K. Bilge, Y. Yorulmaz, F. Javanshour, A. Ürkmez, B. Yılmaz, E. Şimşek, M. Papila, Synergistic role of in-situ crosslinkable electrospun nanofiber/epoxy nanocomposite interlayers for superior laminated composites, Composites Science and Technology. 151 (2017) 310–316. https://doi.org/10.1016/j.compscitech.2017.08.029.
[20] F. Velázquez-Contreras, C. Zamora-Ledezma, I. López-González, L. Meseguer-Olmo, E. Núñez-Delicado, J.A. Gabaldón, Cyclodextrins in Polymer-Based Active Food Packaging: A Fresh Look at Nontoxic, Biodegradable, and Sustainable Technology Trends, Polymers. 14 (2021) 104. https://doi.org/10.3390/polym14010104.
[21] G. El Fawal, Polymer nanofibers electrospinning: A review, Egypt. J. Chem. 0 (2019) 0–0. https://doi.org/10.21608/ejchem.2019.14837.1898.
[22] J. Xue, J. Xie, W. Liu, Y. Xia, Electrospun Nanofibers: New Concepts, Materials, and Applications, Acc. Chem. Res. (2017) 12.
[23] C. Narváez-Muñoz, D.F. Diaz-Suntaxi, L.M. Carrión-Matamoros, V.H. Guerrero, C.E. Almeida-Naranjo, V. Morales-Flórez, A. Debut, K. Vizuete, D.J. Mowbray, C. Zamora-Ledezma, Impact of the solvent composition on the structural and mechanical properties of customizable electrospun poly(vinylpyrrolidone) fiber mats, Phys. Chem. Chem. Phys. 23 (2021) 22923–22935. https://doi.org/10.1039/D1CP03145G.
[24] H. Liao, Y. Wu, M. Wu, H. Liu, Effects of fiber surface chemistry and roughness on interfacial structures of electrospun fiber reinforced epoxy composite films, Polym Compos. 32 (2011) 837–845. https://doi.org/10.1002/pc.21107.
[25] B. De Schoenmaker, S. Van der Heijden, I. De Baere, W. Van Paepegem, K. De Clerck, Effect of electrospun polyamide 6 nanofibres on the mechanical properties of a glass fibre/epoxy composite, Polymer Testing. 32 (2013) 1495–1501. https://doi.org/10.1016/j.polymertesting.2013.09.015.
[26] A. Kausar, A. Iqbal, S.T. Hussain, Preparation and properties of polyamide/ epoxy/multi-walled carbon nanotube nanocomposite, Journal of Plastic Film & Sheeting. 30 (2014) 205–224.
[27] I.D.G.A. Subagia, Z. Jiang, L.D. Tijing, Y. Kim, C.S. Kim, J.K. Lim, K. Shon, Hybrid Multi-scale Basalt Fiber-epoxy Composite Laminate Reinforced with Electrospun Polyurethane Nanofibers Containing Carbon Nanotubes, Fibers and Polymers. 15 (2014) 1295–1302. https://doi.org/10.1007/s12221-014-1295-4.
[28] S. Polat, A. Avcı, M. Ekrem, Fatigue behavior of composite to aluminum single lap joints reinforced with graphene doped nylon 66 nanofibers, Composite Structures. 194 (2018) 624–632. https://doi.org/10.1016/j.compstruct.2018.04.043.
[29] A. Bhargav, K. Min, L. Wen Feng, J.Y.H. Fuh, V. Rosa, Taguchi's methods to optimize the properties and bioactivity of 3D printed polycaprolactone/mineral trioxide aggregate scaffold: Theoretical predictions and experimental validation, J Biomed Mater Res. 108 (2020) 629–637. https://doi.org/10.1002/jbm.b.34417.
[30] R. Ranjit K., Design of Experiments Using The Taguchi Approach 16 Steps to Product and

Process Improvement, 2001.
[31] M. Elkasaby, H.A. Hegab, A. Mohany, G.M. Rizvi, Modeling and optimization of electrospinning of polyvinyl alcohol (PVA), Adv Polym Technol. 37 (2018) 2114–2122. https://doi.org/10.1002/adv.21869.
[32] C. Narváez-Muñoz, P. Ryzhakov, J. Pons-Prats, Determination of the Operational Parameters for the Manufacturing of Spherical PVP Particles via Electrospray, Polymers. 13 (2021) 529. https://doi.org/10.3390/polym13040529.
[33] I.A. Kinloch, J. Suhr, J. Lou, R.J. Young, P.M. Ajayan, Composites with carbon nanotubes and graphene: An outlook, Science. 362 (2018) 547–553. https://doi.org/10.1126/science.aat7439.
[34] C.P. Narváez-Muñoz, L.M. Carrion-Matamoros, K. Vizuete, A. Debut, C.R. Arroyo, V. Guerrero, C.E. Almeida-Naranjo, V. Morales-Flórez, D.J. Mowbray, C. Zamora-Ledezma, Tailoring Organic–Organic Poly(vinylpyrrolidone) Microparticles and Fibers with Multiwalled Carbon Nanotubes for Reinforced Composites, ACS Appl. Nano Mater. 2 (2019) 4302–4312. https://doi.org/10.1021/acsanm.9b00758.
[35] ASTM D3039/D3039M-17, Test Method for Tensile Properties of Polymer Matrix Composite Materials, ASTM International, 2017. https://doi.org/10.1520/D3039_D3039M-14.
[36] E. Uslu, M. Gavgali, M.O. Erdal, Ş. Yazman, L. Gemi, Determination of mechanical properties of polymer matrix composites reinforced with electrospinning N66, PAN, PVA and PVC nanofibers: A comparative study, Materials Today Communications. 26 (2021) 101939. https://doi.org/10.1016/j.mtcomm.2020.101939.
[37] S.S.S. Bakar, K.C. Fong, A. Eleyas, M.F.M. Nazeri, Effect of Voltage and Flow Rate Electrospinning Parameters on Polyacrylonitrile Electrospun Fibers, IOP Conference Series: Materials Science and Engineering. 318 (2018).
[38] D.S. Gomes, A.N.R. da Silva, N.I. Morimoto, L.T.F. Mendes, R. Furlan, I. Ramos, Characterization of an electrospinning process using different PAN/DMF concentrations, Polímeros. 17 (2007) 206–211. https://doi.org/10.1590/S0104-14282007000300009.
[39] R. Jalili, M. Morshed, S.A.H. Ravandi, Fundamental parameters affecting electrospinning of PAN nanofibers as uniaxially aligned fibers, J. Appl. Polym. Sci. 101 (2006) 4350–4357. https://doi.org/10.1002/app.24290.
[40] E. Uslu, M. Gavgali, M.O. Erdal, Ş. Yazman, L. Gemi, Determination of mechanical properties of polymer matrix composites reinforced with electrospinning N66, PAN, PVA and PVC nanofibers: A comparative study, Materials Today Communications. 26 (2021) 101939. https://doi.org/10.1016/j.mtcomm.2020.101939.
[41] S.S.S. Bakar, K.C. Fong, A. Eleyas, M.F.M. Nazeri, Effect of Voltage and Flow Rate Electrospinning Parameters on Polyacrylonitrile Electrospun Fibers, (2017) 7.
[42] M.K. Shin, B. Lee, S.H. Kim, J.A. Lee, G.M. Spinks, S. Gambhir, G.G. Wallace, M.E. Kozlov, R.H. Baughman, S.J. Kim, Synergistic toughening of composite fibres by self-alignment of reduced graphene oxide and carbon nanotubes, Nat Commun. 3 (2012) 650. https://doi.org/10.1038/ncomms1661.
[43] M.A. Wsoo, S. Shahir, S.P. Mohd Bohari, N.H. Mat Nayan, S.I. Abd Razak, A review on the properties of electrospun cellulose acetate and its application in drug delivery systems: A new perspective, Carbohydrate Research. 491 (2020) 107978. https://doi.org/10.1016/j.carres.2020.107978.
[44] A. Keirouz, M. Chung, J. Kwon, G. Fortunato, N. Radacsi, 2D and 3D electrospinning technologies for the fabrication of nanofibrous scaffolds for skin tissue engineering: A review, WIREs Nanomed Nanobiotechnol. 12 (2020). https://doi.org/10.1002/wnan.1626.
[45] M. Haider, P. Hubert, L. Lessard, An experimental investigation of class A surface finish of composites made by the resin transfer molding process, Composites Science and Technology. 67

(2007) 3176–3186. https://doi.org/10.1016/j.compscitech.2007.04.010.
[46] P. Lv, Y. Feng, P. Zhang, H. Chen, N. Zhao, W. Feng, Increasing the interfacial strength in carbon fiber/epoxy composites by controlling the orientation and length of carbon nanotubes grown on the fibers, Carbon. 49 (2011) 4665–4673. https://doi.org/10.1016/j.carbon.2011.06.064.
[47] S.P. Miguel, D.R. Figueira, D. Simões, M.P. Ribeiro, P. Coutinho, P. Ferreira, I.J. Correia, Electrospun polymeric nanofibres as wound dressings: A review, Colloids and Surfaces B: Biointerfaces. 169 (2018) 60–71. https://doi.org/10.1016/j.colsurfb.2018.05.011.
[48] M. Michalska-Sionkowska, M. Walczak, A. Sionkowska, Antimicrobial activity of collagen material with thymol addition for potential application as wound dressing, Polymer Testing. 63 (2017) 360–366. https://doi.org/10.1016/j.polymertesting.2017.08.036.
[49] R. Andrews, M.C. Weisenberger, Carbon nanotube polymer composites, Current Opinion in Solid State and Materials Science. 8 (2004) 31–37. https://doi.org/10.1016/j.cossms.2003.10.006.
[50] P. Rivero-Antúnez, R. Cano-Crespo, L. Esquivias, N. de la Rosa-Fox, C. Zamora-Ledezma, A. Domínguez-Rodríguez, V. Morales-Flórez, Mechanical characterization of sol-gel alumina-based ceramics with intragranular reinforcement of multiwalled carbon nanotubes, Ceramics International. 46 (2020) 19723–19730. https://doi.org/10.1016/j.ceramint.2020.04.285.
[51] V. Morales-Flórez, A. Domínguez-Rodríguez, Mechanical properties of ceramics reinforced with allotropic forms of carbon, Progress in Materials Science. 128 (2022) 100966. https://doi.org/10.1016/j.pmatsci.2022.100966.
[52] R. Wazalwar, M. Sahu, A.M. Raichur, Mechanical properties of aerospace epoxy composites reinforced with 2D nano-fillers: current status and road to industrialization, Nanoscale Adv. 3 (2021) 2741–2776. https://doi.org/10.1039/D1NA00050K.
[53] ISO 1302: 2002, Geometrical Product Specifications (GPS) — Indication of surface texture in technical product documentation, n.d.
[54] V. Eskizeybek, A. Yar, A. Avcı, CNT-PAN hybrid nanofibrous mat interleaved carbon/epoxy laminates with improved Mode I interlaminar fracture toughness, Composites Science and Technology. 157 (2018) 30–39. https://doi.org/10.1016/j.compscitech.2018.01.021.
[55] S. Pathak, G.C. Saha, M.B. Abdul Hadi, N.K. Jain, Engineered Nanomaterials for Aviation Industry in COVID-19 Context: A Time-Sensitive Review, Coatings. 11 (2021) 382. https://doi.org/10.3390/coatings11040382.